

Universal relation between dipole polarizability of finite nuclei and neutron-star compactness

P.S. Koliogiannis^{1,2,*}, T. Ghosh^{1,†}, E. Yüksel^{3,‡} and N. Paar^{1,§}

¹*Department of Physics, Faculty of Science, University of Zagreb, Bijenička cesta 32, 10000, Zagreb, Croatia*

²*Department of Theoretical Physics, Aristotle University of Thessaloniki, 54124 Thessaloniki, Greece* and

³*School of Mathematics and Physics, University of Surrey, Guildford, Surrey, GU2 7XH, United Kingdom*

(Dated: January 26, 2026)

The nuclear equation of state, which determines the structure and properties of neutron stars, remains subject to substantial theoretical uncertainties, leading to model dependence in predicted observables. Universal relations have emerged as a powerful tool to mitigate this dependence by linking neutron star observables in a framework-independent manner. In this work, we introduce a new universal relation that *bridges* finite nuclei and neutron stars through the dimensionless quantity $\zeta = \beta_{1.4} \tilde{L}^{-1}$, which couples the compactness of a $1.4 M_{\odot}$ neutron star to the slope of the nuclear symmetry energy at saturation. The relation is examined under a broad set of relativistic energy density functionals with point-coupling and meson-exchange interactions, as well as non-relativistic Skyrme functionals. We demonstrate that ζ exhibits a strong exponential correlation with the electric dipole polarizability α_D in finite nuclei across all considered equations of state. By exploiting experimental α_D data for selected neutron-rich nuclei, we constrain ζ and translate these constraints into equation-of-state-independent bounds on the neutron star radius $R_{1.4}$ and the symmetry-energy slope L , providing insights into the properties of neutron star matter.

I. INTRODUCTION

Neutron stars serve as natural laboratories for exploring the interplay between nuclear and gravitational physics under the most extreme conditions in the universe. Their cores reach baryonic densities several times greater than the nuclear saturation density—regimes that remain far beyond the reach of terrestrial experiments. The internal structure and macroscopic properties of neutron stars are governed by the equation of state (EOS) of dense matter, which encapsulates the microphysics through the relationship between pressure and energy density. However, substantial uncertainties in the EOS remain, mainly because the density dependence of the nuclear symmetry energy is poorly known at supra-saturation densities, which are essential for neutron star physics [1–3].

Over the past decade, multimessenger observations have imposed increasingly stringent constraints on the dense matter EOS. Precision measurements of massive neutron stars with $M \gtrsim 2 M_{\odot}$ establish a robust lower bound on the stiffness of the EOS [4–8]. Radius estimates from X-ray timing missions, such as NICER, probe the nature of the intermediate density regime [9–14], while gravitational-wave signals from binary mergers, most notably GW170817 and GW190425, encode tidal deformabilities that directly constrain the EOS at supra-nuclear densities [15, 16]. Additional constraints arise from rapid rotation which imposes limits on the maximum mass, radius, moment of inertia, quadrupole moment, and dimensionless spin parameter that any viable EOS must satisfy. In this context, the fastest known pulsar, rotating at 716 Hz, serves as an observational benchmark for these limits [17–19].

Complementary constraints on the EOS arise from nuclear physics experiments that probe various properties of finite nu-

clei [20]. Measurements of neutron skin thickness in heavy nuclei and dipole polarizabilities provide direct sensitivity to the density dependence of the nuclear symmetry energy around saturation density [21–28], as well as at subsaturation densities [29]. In parallel, heavy-ion collision observables offer insights into the pressure of asymmetric matter at supra-saturation densities [30–32]. These measurements, in conjunction with astrophysical constraints, aim to confine the EOS across densities and establish a firm link between finite nuclei and neutron star properties.

In addition to observational and experimental bounds, an important development has been the discovery of universal relations among bulk neutron star properties. Being largely independent of the underlying EOS, these relations enable connections between otherwise inaccessible stellar observables, thereby constrain the behavior of dense matter at supra-nuclear densities. Among these, the I-Love-Q set represents the foundational relation, connecting the moment of inertia, tidal deformability, and quadrupole moment [33–38]. The neutron star binding energy has been shown to obey universal relations with compactness and tidal deformability, providing an additional EOS-insensitive observable for both isolated and binary systems [39–42]. These correlations have been further extended to a wide range of scenarios, including rapidly rotating stars [19, 43–53], finite-temperature stars relevant for mergers [41, 44, 54–56], and hybrid configurations that incorporate additional degrees of freedom such as deconfined quarks or hyperons [33, 55, 57–60]. Universal relations have also been applied to gravitational-wave asteroseismology, allowing oscillation mode frequencies to constrain neutron star masses and radii [61–64]. Furthermore, combining astrophysical observations with nuclear physics-informed quantities has been used to tighten constraints on neutron star bulk properties [35, 65–74]. In binary neutron star systems, universal relations for tidal deformabilities enable gravitational-wave measurements of the inspiral phase to more directly constrain neutron star structure and the equation of state via tidal effects encoded in the waveform [75–77].

* pkoliogi@phy.hr

† tghosh@phy.hr

‡ e.yuksel@surrey.ac.uk

§ npaar@phy.hr

In this work, we introduce a universal relation connecting a finite-nucleus observable—the electric dipole polarizability, α_D —to a key neutron star property, namely the compactness of a canonical $1.4 M_\odot$ neutron star. Both quantities are strongly influenced by the slope of the nuclear symmetry energy at saturation, L , which governs the pressure of neutron-rich matter [20], thereby establishing a direct connection between nuclear experiments and neutron star structure. To explore this relation, we employ a comprehensive set of microscopic nuclear models based on energy density functional (EDF) theory, including relativistic density-dependent point-coupling (DD-PC) [78, 79], density-dependent meson-exchange (DD-ME) [80], and nonlinear meson-exchange (NL) [81, 82] interactions, alongside non-relativistic Skyrme functionals [83]. EDFs provide a unified and self-consistent framework for describing both finite nuclei and neutron stars, capturing bulk nuclear properties and the density dependence of the symmetry energy that are essential for establishing robust nuclear–astrophysical correlations. The resulting universal relation exhibits a remarkably consistent exponential trend across the full set of EOSs and nuclei considered, allowing us to place constraints on neutron star radii and the symmetry energy slope. Furthermore, it serves as a predictive tool for α_D in nuclei where experimental measurements are not yet available. Altogether, this framework provides a direct, largely model-independent bridge between terrestrial nuclear experiments and astrophysical observations, offering a stringent benchmark for the nuclear EOS.

The paper is organized as follows. Section II presents the nuclear models and the corresponding EOSs employed in this work, while Sec. III lays out the followed methodology. Section IV contains the results and their discussion, where we focus on the universal relation, and implications for neutron star and finite nuclei structure. Finally, Sec. V summarizes the main findings and concludes the implications for nuclear and astrophysical observables.

II. NUCLEAR MODELS AND EQUATIONS OF STATE

In this work, we employ a comprehensive set of relativistic and non-relativistic EDFs, which are capable of consistently describing finite nuclei and neutron-star matter. This framework enables a systematic exploration of universal relations linking microscopic nuclear structure to macroscopic stellar properties. Within the relativistic EDFs, we consider several variants of DD-PC [78, 79], DD-ME [80, 84], and NL [81, 82] interactions. The non-relativistic EDFs include Skyrme parameterizations—KDEv01 [85], SGI [86], SK255 and SK272 [87], SLy230a, SLy4, and SLy5 [88, 89], as well as SkI2, SkI3, and SkI5 [90]. In addition, we employ the SAMi-J family of Skyrme functionals [91] (SAMi-J30, SAMi-J32, and SAMi-J34), which is specifically designed to allow a controlled variation of the symmetry-energy slope.

Overall, this study employs EOSs derived from 12 DD-PC, 7 DD-ME, 6 NL, and 13 Skyrme functionals, covering a broad range of nuclear matter properties, including incompressibility $K \sim 211\text{--}356$ MeV, symmetry energy $J \sim 27\text{--}47$ MeV, and its slope $L \sim 19\text{--}140$ MeV. Neutron star matter is described

TABLE I. Properties of the EOSs, including the slope of the symmetry energy (L), the maximum mass (M_{\max}), and the corresponding radius (R_{\max}), and the radius of a $1.4 M_\odot$ neutron star ($R_{1.4}$).

| EOS | L (MeV) | M_{\max} (M_\odot) | R_{\max} (km) | $R_{1.4}$ (km) |
|------------|-----------|--------------------------|-----------------|----------------|
| DD-PC-J29 | 29.00 | 2.20 | 10.61 | 11.81 |
| DD-PC-J30 | 35.60 | 2.20 | 10.63 | 11.92 |
| DD-PC-J31 | 43.80 | 2.19 | 10.63 | 12.00 |
| DD-PC-J32 | 52.30 | 2.19 | 10.63 | 12.08 |
| DD-PC-J33 | 62.00 | 2.18 | 10.63 | 12.21 |
| DD-PC-J34 | 72.10 | 2.17 | 10.65 | 12.38 |
| DD-PC-J35 | 83.20 | 2.17 | 10.71 | 12.62 |
| DD-PC-J36 | 94.10 | 2.17 | 10.83 | 12.90 |
| DD-PC-CREX | 19.60 | 2.09 | 10.06 | 11.26 |
| DD-PC-PREX | 101.78 | 2.07 | 10.44 | 12.75 |
| DD-PC-REX | 30.03 | 2.19 | 10.56 | 11.82 |
| DD-PCX | 46.32 | 2.16 | 10.45 | 11.86 |
| DD-ME-J30 | 30.01 | 2.47 | 11.96 | 12.87 |
| DD-ME-J32 | 46.53 | 2.46 | 11.98 | 13.11 |
| DD-ME-J34 | 62.06 | 2.44 | 11.99 | 13.36 |
| DD-ME-J36 | 85.43 | 2.44 | 12.12 | 13.82 |
| DD-ME-J38 | 110.64 | 2.48 | 12.43 | 14.39 |
| DD-ME1 | 55.43 | 2.44 | 11.94 | 13.22 |
| DD-ME2 | 51.26 | 2.48 | 12.07 | 13.25 |
| NL-SC | 108.31 | 2.64 | 12.75 | 14.44 |
| NL-SH | 113.51 | 2.80 | 13.54 | 14.98 |
| NLC | 139.93 | 2.81 | 13.40 | 14.92 |
| NL1 | 118.45 | 2.77 | 13.34 | 14.85 |
| NL3 | 122.50 | 2.76 | 13.26 | 14.80 |
| NL3* | 107.32 | 2.64 | 12.75 | 14.43 |
| KDEv01 | 54.70 | 1.97 | 9.77 | 11.58 |
| SAMI-J30 | 63.18 | 2.14 | 10.60 | 12.55 |
| SAMI-J32 | 85.10 | 2.18 | 11.01 | 13.27 |
| SAMI-J34 | 105.31 | 2.19 | 11.25 | 13.83 |
| SGI | 63.86 | 2.24 | 10.96 | 12.87 |
| SK255 | 95.05 | 2.14 | 10.86 | 13.23 |
| SK272 | 91.67 | 2.23 | 11.08 | 13.36 |
| SLy230a | 44.32 | 2.11 | 10.30 | 11.90 |
| SLy4 | 45.96 | 2.05 | 9.99 | 11.69 |
| SLy5 | 48.27 | 2.05 | 10.04 | 11.76 |
| SkI2 | 104.33 | 2.16 | 11.17 | 13.70 |
| SkI3 | 100.52 | 2.24 | 11.35 | 13.69 |
| SkI5 | 129.33 | 2.24 | 11.54 | 14.36 |

across two density regimes: (i) the liquid core and (ii) the inner and outer crust. The liquid core consists of neutrons, protons, electrons, and muons in β -equilibrium and charge neutrality. For densities relevant to the crust, we adopt the SLy EOS [92] for the inner crust and the BPS [93] and FMT [94] EOSs for the outer crust, matched to the core EOS at the crust–core transition determined using the thermodynamical method [95, 96].

Table I presents the full set of EOSs used in this work, along with key nuclear matter and neutron star properties, including the slope of the symmetry energy L , the maximum mass M_{\max} , the corresponding radius R_{\max} , and the radius at $1.4 M_\odot$, $R_{1.4}$. All EOSs are calibrated to reproduce the saturation properties of symmetric nuclear matter and support a maximum neutron star mass of at least $2 M_\odot$, in agreement with current astrophysical observations. The wide coverage of EOSs, encompassing both soft and stiff models and predicting $1.4 M_\odot$ radii between

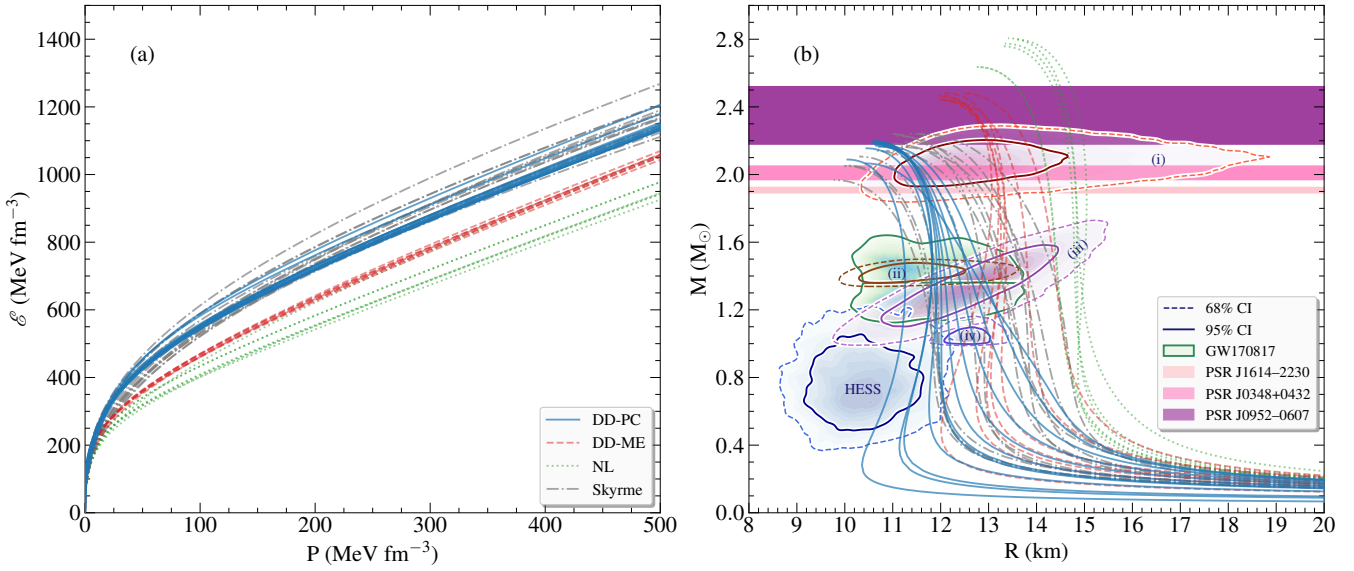


FIG. 1. (a) The energy density as a function of pressure for the full set of EOSs. (b) The corresponding gravitational mass as a function of radius for the full set of EOSs. The shaded contour labeled HESS indicates constraints inferred from the HESS J1731–347 supernova remnant [97]. Additional observational constraints are shown for: (i) PSR J0740+6620 [7, 14], (ii) PSR J0437–4715 [98], (iii) PSR J0030+0451 [10, 11], and (iv) PSR J1231–1411 [99]. Horizontal shaded bands denote mass measurements of the massive pulsars PSR J1614–2230 [4], PSR J0348+0432 [5], and PSR J0952–0607 [8], providing lower bounds on the maximum neutron star mass. Constraints from the binary neutron star merger GW170817 [100] are also indicated.

11 and 15 km, offers a robust framework for testing the proposed universal relation and investigating correlations that are mainly insensitive to the specific stiffness of the EOS. For illustration, the associated energy–pressure and mass–radius relations are shown in Fig. 1, overlaid with up-to-date astrophysical constraints [4–15, 97–100]. Overall, this set provides a comprehensive and systematically constrained framework suitable for investigating correlations between microscopic nuclear observables and macroscopic neutron star properties.

III. METHODOLOGY

To establish a quantitative link between nuclear structure and neutron star properties, we focus on two key observables: (a) the electric dipole polarizability, α_D , a sensitive isovector observable characterizing the nuclear response to an external electric field [23, 101], and (b) the stellar compactness, β , which encodes the interplay between gravitational mass and radius of neutron stars.

The electric dipole polarizability α_D is defined as the inverse energy-weighted sum of the isovector dipole response in finite nuclei, largely governed by the isovector giant dipole resonance, a collective oscillation of neutrons against protons [20, 102, 103]. It is calculated as

$$\alpha_D = \frac{8\pi e^2}{9} \int_0^\infty E^{-1} S(E1; E) dE, \quad (1)$$

where $S(E1; E)$ denotes the electric dipole strength as a function of the excitation energy E , obtained using the quasiparticle

random phase approximation in both relativistic [102, 104] and non-relativistic frameworks [105, 106]. On the other hand, stellar compactness β is a dimensionless quantity characterizing the neutron star and is defined as

$$\beta = \frac{GM}{c^2 R}, \quad (2)$$

where M and R denote the gravitational mass and the radius, respectively. Both dipole polarizability α_D and stellar compactness β are strongly governed by the density dependence of the symmetry energy slope, L , which acts as a natural mediator connecting nuclear and stellar properties: α_D correlates directly with L (see also Refs. [101, 107]), while β reflects its influence via the neutron star radius. In particular, the well-established correlation between $R_{1.4}$ and the pressure of neutron star matter up to $\sim 2\rho_0$ [39], extended to $R_{1.4}$ and L [83], ensures that L provides a link across the relevant density regimes.

To formalize this connection, we introduce a dimensionless quantity

$$\zeta \equiv \beta_{1.4} \tilde{L}^{-1}, \quad (3)$$

where $\beta_{1.4}$ denotes the compactness of a $1.4 M_\odot$ neutron star, and $\tilde{L} = L/L_0$ with $L_0 = 100$ MeV as a reference value. The ratio ζ effectively characterizes the stiffness of the EOS: lower values correspond to stiffer models with greater pressure support, where the L and $R_{1.4}$ values are higher, whereas higher values indicate softer behavior. Specifically, L probes the EOS near saturation density ρ_0 , while $\beta_{1.4}$ captures the influence of the symmetry energy slope at densities $\sim (2-3)\rho_0$ through its dependence on $R_{1.4}$, which can be related to saturation density

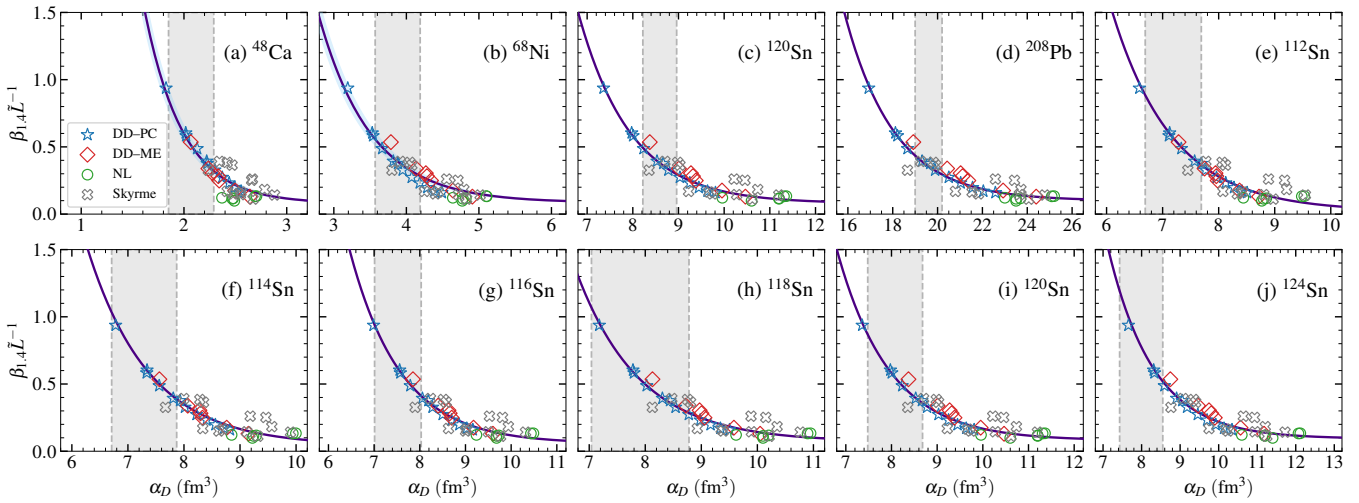


FIG. 2. The dimensionless quantity $\zeta \equiv \beta_{1.4} \tilde{L}^{-1}$ as a function of the electric dipole polarizability α_D for the full set of EOSs. Vertical shaded regions indicate experimental values of α_D for: (a) ^{48}Ca [21], (b) ^{68}Ni [22], (c) ^{120}Sn [23, 26], (d) ^{208}Pb [23, 24], and (e–j) $^{112-124}\text{Sn}$ [27]. The solid curve represents the universal relation (4), with the shaded band indicating its associated uncertainty.

using experimental data from finite nuclei [15]. Since $\beta_{1.4}$ and L probe complementary density regimes, their combination provides a physically motivated bridge between neutron star structure and finite nuclei, establishing ζ as a natural candidate for exploring universal correlations with the electric dipole polarizability, α_D .

IV. RESULTS AND DISCUSSION

A. A universal finite nuclei - neutron star relation

Figure 2 illustrates the dimensionless quantity ζ as a function of the electric dipole polarizability α_D for the full set of EOSs, as well as for ten neutron-rich nuclei for which experimental α_D values are available: ^{48}Ca [21], ^{68}Ni [22], ^{120}Sn [23, 26], ^{208}Pb [23, 24], and even-even isotopes $^{112-124}\text{Sn}$ [27]. Despite their different theoretical foundations, all EOS-models follow a general trend, revealing an EOS-insensitive correlation between dipole polarizability and neutron-star compactness, driven primarily by the symmetry energy slope. We find that this trend is well reproduced by the following empirical exponential relation, chosen as a simple functional form that accurately captures the observed nonlinear behavior over the full range of α_D values considered:

$$\zeta(\alpha_D, A, \delta) = c_1(A) e^{-c_2(A)\alpha_D} + c_3(\delta), \quad (4)$$

where the coefficients c_i ($i = 1 - 3$) depend on the nuclear mass number A and the isospin asymmetry $\delta = (N - Z)/A$, with N and Z denoting the neutron and proton numbers, respectively. These coefficients encode mass and isospin systematics relevant to both finite nuclei and neutron-star properties. Here,

we introduce the following expansions of the coefficients,

$$c_1(A) = \sum_{k=0}^3 q_{1k} A^{-k}, \quad (5)$$

$$c_2(A) = \sum_{k=0}^3 q_{2k} A^{-k}, \quad (6)$$

$$c_3(\delta) = \sum_{k=0}^3 q_{3k} \delta^k. \quad (7)$$

The expansions in Eqs. (5)–(7) are truncated at $k = 3$, a choice that balances accuracy with simplicity by providing an excellent description of the nuclear and neutron star data without introducing unnecessary fit parameters. The inverse-power dependence on A captures the smooth mass variation of bulk nuclear properties, while the polynomial dependence on δ accounts for residual isospin effects. Truncation at higher-order terms, $k > 3$, do not yield appreciable improvement, ensuring a stable and robust parametrization.

Although Fig. 2 displays results only for nuclei with measured α_D values to avoid redundancy, the fit, given by Eq. (4), was performed using a broader training set of fourteen nuclei: ^{48}Ca , ^{54}Ca , ^{60}Ca , ^{86}Kr , ^{68}Ni , ^{78}Ni , ^{208}Pb , $^{112-124}\text{Sn}$, and ^{96}Zr , spanning a wide range in nuclear mass number ($A \sim 48-208$) and isospin asymmetry ($\delta \sim 0.11-0.33$). The resulting regression achieves a global coefficient of determination $R^2 \gtrsim 0.9$, indicating that the relation reliably describes both light and heavy nuclei. The extracted expansion coefficients q_{ik} , with $i = 1-3$, are listed in Table II.

B. Neutron star constraints

The existence of the universal relation given in Eq. (4), alongside with the precise experimental measurements of the elec-

TABLE II. Coefficients of the expansions in Eqs. (5)–(7) that appear in Eq. (4).

| Coefficients | q_{1k} | q_{2k} (fm $^{-3}$) | q_{3k} |
|--------------|----------------------|------------------------|----------|
| $k = 0$ | 5.558×10^3 | -0.770 | -0.257 |
| $k = 1$ | -1.080×10^6 | 3.666×10^2 | 3.993 |
| $k = 2$ | 6.909×10^7 | -2.749×10^4 | -15.288 |
| $k = 3$ | -1.432×10^9 | 8.540×10^5 | 20.714 |

tric dipole polarizability α_D in ten neutron-rich nuclei [21–24, 26, 27], indicated by the vertical shaded bands in Fig. 2, allows us to impose quantitative bounds on the dimensionless quantity ζ . To this end, we follow the procedure introduced in Ref. [101], in which the nuclei are divided into two subsets in order to account for differences in the completeness and reliability of the experimental dipole response.

Specifically, the first subset, denoted CNSP-4, consists of ^{48}Ca , ^{68}Ni , ^{120}Sn , and ^{208}Pb , for which α_D has been extracted with minimal theoretical input. The second subset, CNSP-10, extends this selection by including the even-even Sn isotopes 112 – ^{124}Sn , thereby providing a broader experimental basis. For these isotopes, however, contributions to α_D above 20 MeV are reconstructed using quasiparticle–phonon model calculations [27], introducing an additional level of model dependence. Recent analyses indicate that these reconstructed strengths tend to favor lower values of the symmetry energy compared to those inferred from other nuclei, resulting in a mild tension with existing constraints. For this reason, CNSP-4 is regarded as the more conservative and reliable set for neutron star applications, although results obtained using CNSP-10 are also reported for completeness (see Ref. [101] for a detailed discussion).

Using the nuclei in each subset, we calculate weighted averages of ζ , obtaining

$$\text{CNSP-4} : \quad \zeta = 0.390 \pm 0.052, \quad (8)$$

$$\text{CNSP-10} : \quad \zeta = 0.435 \pm 0.047. \quad (9)$$

These bounds delineate the region permitted by the interplay between the compactness of a $1.4 M_\odot$ neutron star and the slope of the symmetry energy. The higher ζ value obtained for CNSP-10 reflects its tendency toward smaller symmetry-energy slopes, consistent with the discussion above.

While ζ encapsulates the interplay between nuclear and neutron-star physics in a compact and model-independent form, its physical content can be further explored through its constituents, the neutron-star radius $R_{1.4}$ and the slope of the symmetry energy L . Guided by the bounds on ζ , we therefore derive corresponding constraints on the product $R_{1.4}L$. In particular, we find

$$\text{CNSP-4} : \quad R_{1.4}L = 554.4 \pm 73.4 \text{ (km MeV)}, \quad (10)$$

$$\text{CNSP-10} : \quad R_{1.4}L = 440.6 \pm 47.9 \text{ (km MeV)}, \quad (11)$$

which define two experimentally informed bands that overlap within a relatively narrow region. Although these products do not uniquely determine $R_{1.4}$ without independent information on L , they nevertheless impose nontrivial constraints that any

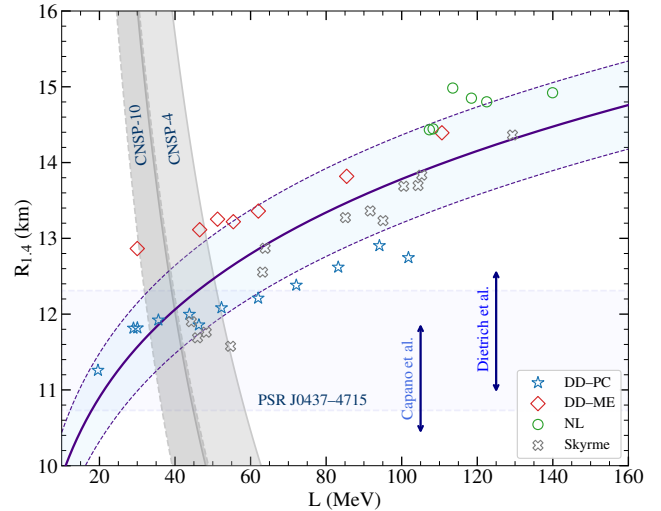


FIG. 3. The radius of a canonical $1.4 M_\odot$ neutron star, $R_{1.4}$, as a function of the slope of the symmetry energy L for the full set of EOSs. Curved shaded regions indicate constraints inferred from the CNSP-4 and CNSP-10 sets of nuclei. The solid curve shows the systematic trend described by Eq. (12), with the associated uncertainty represented by the shaded band. Vertical arrows denote neutron-star radius constraints from Refs. [108, 109], while the horizontal shaded region indicates the radius of PSR J0437–4715 [98].

TABLE III. Constraints on neutron star properties derived from the CNSP-4 and CNSP-10 sets of nuclei. The values correspond to the ranges obtained for the radius of a $1.4 M_\odot$ neutron star ($R_{1.4}$) and the slope of the symmetry energy (L).

| Nuclei set | $R_{1.4}$ (km) | | L (MeV) | |
|------------|----------------------------|----------------------------|----------------------------|----------------------------|
| | min | max | min | max |
| CNSP-4 | $12.057^{+0.505}_{-0.508}$ | $12.472^{+0.505}_{-0.508}$ | $39.896^{+1.615}_{-1.746}$ | $50.335^{+1.972}_{-2.126}$ |
| CNSP-10 | $11.750^{+0.505}_{-0.509}$ | $12.080^{+0.505}_{-0.508}$ | $33.418^{+1.386}_{-1.502}$ | $40.437^{+1.633}_{-1.766}$ |

viable EOS must satisfy. In this sense, the quantity $R_{1.4}L$ emerges as a nuclear-physics–informed consistency criterion for neutron star models.

Figure 3 displays $R_{1.4}$ as a function of the symmetry energy slope L for the full set of EOSs. As mentioned in Sec. III, we also denote the high-degree correlation of $R_{1.4}$ and L , expressed as

$$R_{1.4} = 7.049(L/\text{MeV})^{0.146} \pm 0.581 \text{ (km)}. \quad (12)$$

In addition, we overlay the α_D –informed constraints, CNSP-4 and CNSP-10 from Eqs. (10) and (11), respectively. As these bands serve as a consistency criterion for neutron stars, their intersection with Eq. (12) defines the corresponding bounds on both $R_{1.4}$ and L , shown in Table III.

The two constraint bands reflect not only the experimental uncertainties but also the differing physical implications associated with each nuclear set. The CNSP-4 set, which relies exclusively on measured dipole strength distributions, favors moderately larger radii and symmetry energy slopes. In contrast, the CNSP-10 set, influenced by the model-dependent treat-

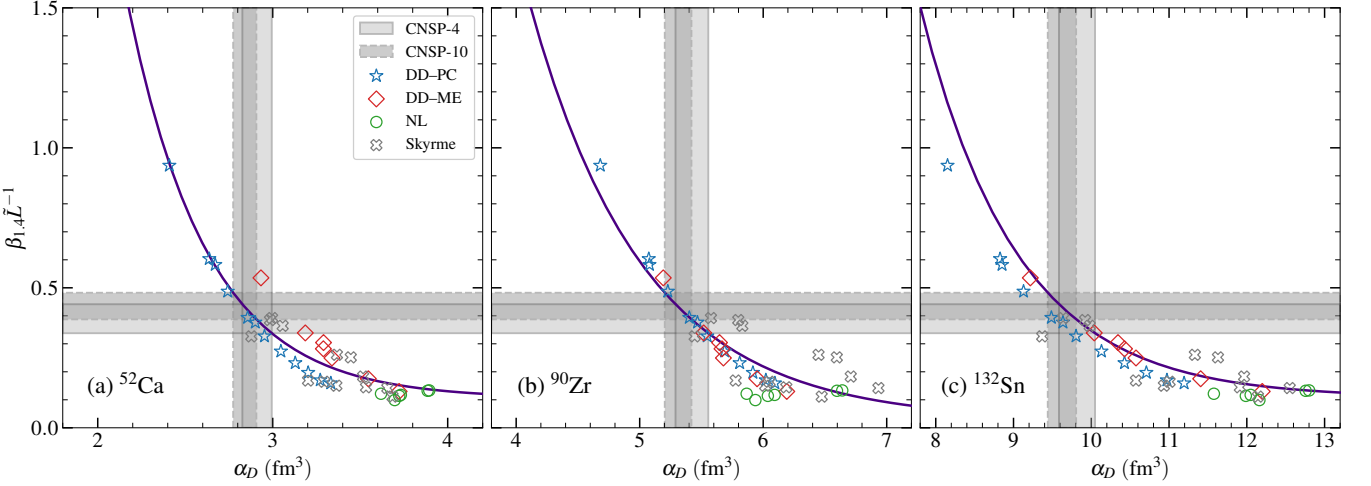


FIG. 4. The dimensionless quantity $\zeta \equiv \beta_{1.4} \tilde{L}$ as a function of the electric dipole polarizability α_D for the full set of EOSs, shown for (a) ^{52}Ca , (b) ^{90}Zr , and (c) ^{132}Sn . The solid curve represents the universal relation (4), with the associated uncertainty indicated by the shaded band. Horizontal shaded regions indicate constraints inferred from the CNSP-4 and CNSP-10 sets of nuclei, while vertical shaded regions indicate the corresponding bounds on the dipole polarizability.

ment of high-energy dipole strength in the Sn isotopes, leads to systematically smaller values of $R_{1.4}$ and L . This distinction highlights the sensitivity of neutron star constraints to the details of the nuclear dipole response and indicates that future high-precision measurements of α_D , particularly in medium and heavy nuclei, will play an important role in further reducing the associated uncertainties.

C. Predictions of α_D for a set of finite nuclei

An important consequence of first establishing the universal relation in Eq. (4) and then constraining the dimensionless quantity ζ is its predictive power. Once experimental data bound ζ , the relation can be inverted to predict the electric dipole polarizability α_D of finite nuclei for which direct measurements are not yet available.

In this work, we focus on three nuclei for which experimental measurements of the electric dipole polarizability are not yet available: ^{52}Ca , ^{90}Zr , and ^{132}Sn . These nuclei were not included in the construction of Eq. (4) and span a wide range of nuclear masses and isospin asymmetries. They probe different shell closures and exhibit distinct pairing characteristics, providing a stringent test of the predictive power of the proposed universal relation in regions of the nuclear chart not constrained by experimental input. In particular,

- (a) ^{52}Ca : a neutron-rich nucleus with a subshell closure at $N = 32$, exhibiting enhanced shell effects and sensitivity to the symmetry energy in the low-mass region. Its emerging magicity makes it an excellent test case for isovector properties.
- (b) ^{90}Zr : an intermediate-mass nucleus with moderate isospin asymmetry and a well-characterized structure,

TABLE IV. Dipole polarizability values and their uncertainty for ^{52}Ca , ^{90}Zr , and ^{132}Sn , as predicted from Eq. (4).

| | Nuclei | α_D (fm³) | σ (fm³) |
|---------|-------------------|------------------|----------------|
| CNSP-4 | ^{52}Ca | 2.911 | 0.084 |
| | ^{90}Zr | 5.423 | 0.133 |
| | ^{132}Sn | 9.816 | 0.231 |
| CNSP-10 | ^{52}Ca | 2.840 | 0.066 |
| | ^{90}Zr | 5.311 | 0.108 |
| | ^{132}Sn | 9.623 | 0.182 |

serving as a benchmark for the universal relation in a different mass region.

- (c) ^{132}Sn : a doubly magic, neutron-rich nucleus with large isospin asymmetry, providing a stringent benchmark for testing EOS predictions in heavier systems strongly influenced by symmetry-energy effects.

Figure 4 shows ζ as a function of the electric dipole polarizability α_D for the three selected nuclei. The horizontal shaded bands indicate the CNSP-4 and CNSP-10 constraints, while the exponential curves correspond to the universal relation given in Eq. (4) for each nucleus. The intersections of the horizontal constraints with the universal curves yield predictions for α_D , which are highlighted by the vertical shaded bands. The corresponding values and uncertainties are summarized in Table IV.

For comparison, we also overlay microscopic EDF-based calculations of α_D for each nucleus. In all cases, the predicted values fall within the range spanned by the microscopic model results. This agreement demonstrates that the universal relation not only captures the global trends across the calibrated functionals, but also exhibits predictive capability for neutron-rich nuclei not included in the fitting procedure.

V. CONCLUSION

This study establishes a universal relation bridging finite nuclei and neutron stars, in which the electric dipole polarizability α_D is linked to the compactness of $1.4 M_\odot$ neutron star, mediated by the slope of the symmetry energy. Both quantities serve as complementary probes of the density dependence of the nuclear symmetry energy, with α_D reflecting nuclear structure and $\beta_{1.4}$ capturing neutron star properties. The emergence of this relation reveals a fundamental connection between microscopic nuclear properties and macroscopic neutron star structure, providing a robust, EOS-insensitive framework that unites laboratory measurements with astrophysical observations. This framework possesses a twofold predictive power: it enables informed predictions of nuclear observables in unexplored regions of the nuclear chart and, simultaneously, translates nuclear constraints into quantitative bounds on neutron star radii and the slope of the symmetry energy.

As experimental determinations of α_D extend to increasingly neutron-rich isotopes and astrophysical observations achieve higher precision, this framework can be further refined to yield tighter constraints on the density dependence of the symmetry energy and neutron star structure. In this way, the present work progress the connection between nuclear and neutron star matter, grounded in shared isovector properties of finite nuclei and supported by both theoretical modeling and experimental data, highlighting the link between terrestrial nuclei and one of the densest astrophysical objects in the universe.

ACKNOWLEDGMENTS

This work is supported by the Croatian Science Foundation under the project number HRZZ-MOBDOL-12-2023-6026 and under the project Relativistic Nuclear Many-Body Theory in the Multimessenger Observation Era (HRZZ-IP-2022-10-7773). E.Y. acknowledges support from the UK STFC under award no. ST/Y000358/1. N.P. acknowledges support from the project “Implementation of cutting-edge research and its application as part of the Scientific Center of Excellence for Quantum and Complex Systems, and Representations of Lie Algebras”, Grant No. PK.1.1.10.0004, co-financed by the European Union through the European Regional Development Fund - Competitiveness and Cohesion Programme 2021-2027.

AUTHOR CONTRIBUTION

The conceptual framework of the study was developed by P.S.K. and N.P. Methodological design and computational implementation were carried out by P.S.K. and N.P., with P.S.K. responsible for model validation, formal analysis, visualization, and figure preparation. Model calculations and data collection and curation were performed by P.S.K., E.Y., and T.G. The manuscript was drafted by P.S.K., and revised by all authors. Supervision and project coordination were provided by N.P. Financial support for this work was secured by P.S.K., E.Y., and N.P.

[1] J. M. Lattimer and M. Prakash, The physics of neutron stars, *Sci.* **304**, 536 (2004).

[2] J. Lattimer, Neutron Stars and the Nuclear Matter Equation of State, *Ann. Rev. Nucl. Part. Sci.* **71**, 433 (2021).

[3] G. Burgio, H.-J. Schulze, I. Vidaña, and J.-B. Wei, Neutron stars and the nuclear equation of state, *Prog. Part. Nucl. Phys.* **120**, 103879 (2021).

[4] Z. Arzoumanian *et al.*, The NANOGrav 11-year Data Set: High-precision Timing of 45 Millisecond Pulsars, *Astrophys. J. Suppl. S.* **235**, 37 (2018).

[5] J. Antoniadis *et al.*, A Massive Pulsar in a Compact Relativistic Binary, *Sci.* **340**, 1233232 (2013).

[6] H. Cromartie *et al.*, Relativistic Shapiro delay measurements of an extremely massive millisecond pulsar, *Nat. Astron.* **4**, 72 (2020).

[7] E. Fonseca *et al.*, Refined Mass and Geometric Measurements of the High-mass PSR J0740+6620, *Astrophys. J. Lett.* **915**, L12 (2021).

[8] R. W. Romani, D. Kandel, A. V. Filippenko, T. G. Brink, and W. Zheng, PSR J0952-0607: The Fastest and Heaviest Known Galactic Neutron Star, *Astrophys. J. Lett.* **934**, L17 (2022).

[9] M. C. Miller *et al.*, PSR J0030+0451 Mass and Radius from NICER Data and Implications for the Properties of Neutron Star Matter, *Astrophys. J. Lett.* **887**, L24 (2019).

[10] T. E. Riley *et al.*, A NICER View of PSR J0030+0451: Millisecond Pulsar Parameter Estimation, *Astrophys. J. Lett.* **887**, L21 (2019).

[11] G. Raaijmakers *et al.*, A NICER View of PSR J0030+0451: Implications for the Dense Matter Equation of State, *Astrophys. J. Lett.* **887**, L22 (2019).

[12] M. C. Miller *et al.*, The Radius of PSR J0740+6620 from NICER and XMM-Newton Data, *Astrophys. J. Lett.* **918**, L28 (2021).

[13] T. E. Riley *et al.*, A NICER View of the Massive Pulsar PSR J0740+6620 Informed by Radio Timing and XMM-Newton Spectroscopy, *Astrophys. J. Lett.* **918**, L27 (2021).

[14] A. J. Dittmann *et al.*, A More Precise Measurement of the Radius of PSR J0740+6620 Using Updated NICER Data, *Astrophys. J.* **974**, 295 (2024).

[15] F. J. Fattoyev, J. Piekarewicz, and C. J. Horowitz, Neutron Skins and Neutron Stars in the Multimessenger Era, *Phys. Rev. Lett.* **120**, 172702 (2018).

[16] B. P. Abbott *et al.*, GW190425: Observation of a Compact Binary Coalescence with Total Mass $\sim 3.4 M_\odot$, *Astrophys. J. Lett.* **892**, L3 (2020).

[17] J. W. T. Hessels, S. M. Ransom, I. H. Stairs, P. C. C. Freire, V. M. Kaspi, and F. Camilo, A Radio Pulsar Spinning at 716 Hz, *Sci.* **311**, 1901 (2006).

[18] M. Bejger, T. Bulik, and P. Haensel, Constraints on the dense matter equation of state from the measurements of PSR J0737-3039A moment of inertia and PSR J0751+1807 mass, *Mon. Not. Roy. Astron. Soc.* **364**, 635 (2005).

[19] P. S. Koliogiannis and C. C. Moustakidis, Effects of the equation of state on the bulk properties of maximally rotating neutron stars, *Phys. Rev. C* **101**, 015805 (2020).

[20] X. Roca-Maza and N. Paar, Nuclear equation of state from ground and collective excited state properties of nuclei, *Prog. Part. Nucl. Phys.* **101**, 96 (2018).

[21] J. Birkhan *et al.*, Electric Dipole Polarizability of ^{48}Ca and Implications for the Neutron Skin, *Phys. Rev. Lett.* **118**, 252501 (2017).

[22] D. M. Rossi *et al.*, Measurement of the Dipole Polarizability of the Unstable Neutron-Rich Nucleus ^{68}Ni , *Phys. Rev. Lett.* **111**, 242503 (2013).

[23] X. Roca-Maza, X. Viñas, M. Centelles, B. K. Agrawal, G. Colò, N. Paar, J. Piekarewicz, and D. Vretenar, Neutron skin thickness from the measured electric dipole polarizability in ^{68}Ni , ^{120}Sn , and ^{208}Pb , *Phys. Rev. C* **92**, 064304 (2015).

[24] A. Tamii *et al.*, Complete Electric Dipole Response and the Neutron Skin in ^{208}Pb , *Phys. Rev. Lett.* **107**, 062502 (2011).

[25] J. Piekarewicz, B. K. Agrawal, G. Colò, W. Nazarewicz, N. Paar, P.-G. Reinhard, X. Roca-Maza, and D. Vretenar, Electric dipole polarizability and the neutron skin, *Phys. Rev. C* **85**, 041302 (2012).

[26] T. Hashimoto *et al.*, Dipole polarizability of ^{120}Sn and nuclear energy density functionals, *Phys. Rev. C* **92**, 031305 (2015).

[27] S. Bassauer *et al.*, Evolution of the dipole polarizability in the stable tin isotope chain, *Phys. Lett. B* **810**, 135804 (2020).

[28] I. Brandherm *et al.*, Electric dipole polarizability of ^{58}Ni , *Phys. Rev. C* **111**, 024312 (2025).

[29] Z. Zhang and L.-W. Chen, Electric dipole polarizability in ^{208}Pb as a probe of the symmetry energy and neutron matter around $\rho_0/3$, *Phys. Rev. C* **92**, 031301 (2015).

[30] P. Russotto *et al.*, Results of the ASY-EOS experiment at GSI: The symmetry energy at suprasaturation density, *Phys. Rev. C* **94**, 034608 (2016).

[31] A. Le Fèvre, Y. Leifels, W. Reisdorf, J. Aichelin, and C. Hartnack, Constraining the nuclear matter equation of state around twice saturation density, *Nucl. Phys. A* **945**, 112 (2016).

[32] S. Huth *et al.*, Constraining neutron-star matter with microscopic and macroscopic collisions, *Nat.* **606**, 276 (2022).

[33] K. Yagi and N. Yunes, I-Love-Q: Unexpected Universal Relations for Neutron Stars and Quark Stars, *Sci.* **341**, 365 (2013).

[34] A. Maselli, V. Cardoso, V. Ferrari, L. Gualtieri, and P. Pani, Equation-of-state-independent relations in neutron stars, *Phys. Rev. D* **88**, 023007 (2013).

[35] K. Yagi and N. Yunes, I-Love-Q relations in neutron stars and their applications to astrophysics, gravitational waves, and fundamental physics, *Phys. Rev. D* **88**, 023009 (2013).

[36] S. Chakrabarti, T. Delsate, N. Gürlebeck, and J. Steinhoff, I-Q Relation for Rapidly Rotating Neutron Stars, *Phys. Rev. Lett.* **112**, 201102 (2014).

[37] N. Jiang and K. Yagi, Analytic I-Love-C relations for realistic neutron stars, *Phys. Rev. D* **101**, 124006 (2020).

[38] T. Lowrey, K. Yagi, and N. Yunes, Improved analytic Love-C relations for neutron stars, *Phys. Rev. D* **111**, 024075 (2025).

[39] J. M. Lattimer and M. Prakash, Neutron Star Structure and the Equation of State, *Astrophys. J.* **550**, 426 (2001).

[40] B. Reed and C. J. Horowitz, Total energy in supernova neutrinos and the tidal deformability and binding energy of neutron stars, *Phys. Rev. D* **102**, 103011 (2020).

[41] P. Laskos-Patkos, P. S. Koliogiannis, A. Kanakis-Pegios, and C. C. Moustakidis, Thermodynamics of Hot Neutron Stars and Universal Relations, *Universe* **8**, 395 (2022).

[42] J. M. Lattimer and M. Prakash, Neutron star observations: Prognosis for equation of state constraints, *Phys. Rep.* **442**, 109 (2007), the Hans Bethe Centennial Volume 1906-2006.

[43] D. D. Doneva, S. S. Yazadjiev, N. Stergioulas, and K. D. Kokkotas, Breakdown of I-Love-Q Universality in Rapidly Rotating Relativistic Stars, *Astrophys. J. Lett.* **781**, L6 (2013).

[44] G. Martinon, A. Maselli, L. Gualtieri, and V. Ferrari, Rotating protoneutron stars: Spin evolution, maximum mass, and I-Love-Q relations, *Phys. Rev. D* **90**, 064026 (2014).

[45] C. Breu and L. Rezzolla, Maximum mass, moment of inertia and compactness of relativistic stars, *Mon. Not. Roy. Astron. Soc.* **459**, 646 (2016).

[46] F. Cipolletta, C. Cherubini, S. Filippi, J. A. Rueda, and R. Ruffini, Last stable orbit around rapidly rotating neutron stars, *Phys. Rev. D* **96**, 024046 (2017).

[47] S.-S. Luk and L.-M. Lin, Universal Relations for Innermost Stable Circular Orbits around Rapidly Rotating Neutron Stars, *Astrophys. J.* **861**, 141 (2018).

[48] R. Riahi, S. Z. Kalantari, and J. A. Rueda, Universal relations for the keplerian sequence of rotating neutron stars, *Phys. Rev. D* **99**, 043004 (2019).

[49] W. Sun, D. Wen, and J. Wang, New quasimassive relations for static and rapid rotating neutron stars, *Phys. Rev. D* **102**, 023039 (2020).

[50] H. O. Silva, G. Pappas, N. Yunes, and K. Yagi, Surface of rapidly-rotating neutron stars: Implications to neutron star parameter estimation, *Phys. Rev. D* **103**, 063038 (2021).

[51] G. Papigiotis and G. Pappas, Universal relations for rapidly rotating neutron stars using supervised machine-learning techniques, *Phys. Rev. D* **107**, 103050 (2023).

[52] C. Musolino, C. Ecker, and L. Rezzolla, On the Maximum Mass and Oblateness of Rotating Neutron Stars with Generic Equations of State, *Astrophys. J.* **962**, 61 (2024).

[53] P. Manoharan and K. D. Kokkotas, Finding universal relations using statistical data analysis, *Phys. Rev. D* **109**, 103033 (2024).

[54] M. Marques, M. Oertel, M. Hempel, and J. Novak, New temperature dependent hyperonic equation of state: Application to rotating neutron star models and I-Q relations, *Phys. Rev. C* **96**, 045806 (2017).

[55] A. R. Raduta, M. Oertel, and A. Sedrakian, Proto-neutron stars with heavy baryons and universal relations, *Mon. Not. Roy. Astron. Soc.* **499**, 914 (2020).

[56] S. Khadkikar, A. R. Raduta, M. Oertel, and A. Sedrakian, Maximum mass of compact stars from gravitational wave events with finite-temperature equations of state, *Phys. Rev. C* **103**, 055811 (2021).

[57] K. Yagi and N. Yunes, Approximate universal relations for neutron stars and quark stars, *Phys. Rep.* **681**, 1 (2017).

[58] J.-B. Wei, A. Figura, G. F. Burgio, H. Chen, and H.-J. Schulze, Neutron star universal relations with microscopic equations of state, *J. Phys. G: Nucl. Part. Phys.* **46**, 034001 (2019).

[59] N. Khosravi Largani, T. Fischer, A. Sedrakian, M. Cierniak, D. E. Alvarez-Castillo, and D. B. Blaschke, Universal relations for rapidly rotating cold and hot hybrid stars, *Mon. Not. Roy. Astron. Soc.* **515**, 3539 (2022).

[60] A. Kumar, M. K. Ghosh, P. Thakur, V. B. Thapa, K. K. Nath, and M. Sinha, Universal relations for compact stars with exotic degrees of freedom, *Eur. Phys. J. C* **84**, 692 (2024).

[61] N. Andersson and K. D. Kokkotas, Gravitational Waves and Pulsating stars: What Can We Learn from Future Observations?, *Phys. Rev. Lett.* **77**, 4134 (1996).

[62] N. Andersson and K. D. Kokkotas, Towards gravitational wave asteroseismology, *Mon. Not. Roy. Astron. Soc.* **299**, 1059 (1998).

[63] D. D. Doneva, E. Gaertig, K. D. Kokkotas, and C. Krüger, Gravitational wave asteroseismology of fast rotating neutron stars with realistic equations of state, *Phys. Rev. D* **88**, 044052 (2013).

[64] G. Lioutas, A. Bauswein, and N. Stergioulas, Frequency deviations in universal relations of isolated neutron stars and postmerger remnants, *Phys. Rev. D* **104**, 043011 (2021).

[65] K. Yagi and N. Yunes, Approximate universal relations among tidal parameters for neutron star binaries, *Class. Quantum Grav.* **34**, 015006 (2016).

[66] B. Kumar and P. Landry, Inferring neutron star properties from GW170817 with universal relations, *Phys. Rev. D* **99**, 123026 (2019).

[67] J. A. Saes and R. F. P. Mendes, Equation-of-state-insensitive measure of neutron star stiffness, *Phys. Rev. D* **106**, 043027 (2022).

[68] K. K. Nath, R. Mallick, and S. Chatterjee, I-Love-Q relations for a generic family of neutron star equations of state, *Mon. Not. Roy. Astron. Soc.* **524**, 1438 (2023).

[69] B. K. Pradhan, A. Vijaykumar, and D. Chatterjee, Impact of updated multipole love numbers and f -Love universal relations in the context of binary neutron stars, *Phys. Rev. D* **107**, 023010 (2023).

[70] E. Aranguren, J. A. Font, N. Sanchis-Gual, and R. Vera, Revisiting the I -Love- Q relations for superfluid neutron stars, *Phys. Rev. D* **108**, 104065 (2023).

[71] J. A. Saes, R. F. P. Mendes, and N. Yunes, Approximately universal I-Love- $\langle c_s^2 \rangle$ relations for the average neutron star stiffness, *Phys. Rev. D* **110**, 024011 (2024).

[72] L. Suleiman and J. Read, Quasiuniversal relations in the context of future neutron star detections, *Phys. Rev. D* **109**, 103029 (2024).

[73] I. Legred, B. O. Sy-Garcia, K. Chatzioannou, and R. Essick, Assessing equation of state-independent relations for neutron stars with nonparametric models, *Phys. Rev. D* **109**, 023020 (2024).

[74] S. Chatterjee and K. K. Nath, Insights into neutron stars from gravitational redshifts and universal relations, *Eur. Phys. J. C* **85**, 862 (2025).

[75] P. Manoharan, C. J. Krüger, and K. D. Kokkotas, Universal relations for binary neutron star mergers with long-lived remnants, *Phys. Rev. D* **104**, 023005 (2021).

[76] D. A. Godzieba, R. Gamba, D. Radice, and S. Bernuzzi, Updated universal relations for tidal deformabilities of neutron stars from phenomenological equations of state, *Phys. Rev. D* **103**, 063036 (2021).

[77] Y. Xie, D. Chatterjee, G. Holder, D. E. Holz, S. Perkins, K. Yagi, and N. Yunes, Breaking bad degeneracies with love relations: Improving gravitational-wave measurements through universal relations, *Phys. Rev. D* **107**, 043010 (2023).

[78] E. Yüksel, T. Oishi, and N. Paar, Nuclear Equation of State in the Relativistic Point-Coupling Model Constrained by Excitations in Finite Nuclei, *Universe* **7**, 71 (2021).

[79] P. Koliogiannis, E. Yüksel, and N. Paar, Constraining neutron star properties through parity-violating electron scattering experiments and relativistic point coupling interactions, *Phys. Lett. B* **862**, 139362 (2025).

[80] D. Vretenar, T. Nikšić, and P. Ring, A microscopic estimate of the nuclear matter compressibility and symmetry energy in relativistic mean-field models, *Phys. Rev. C* **68**, 024310 (2003).

[81] P.-G. Reinhard, M. Rufa, J. Maruhn, W. Greiner, and J. Friedrich, Nuclear ground-state properties in a relativistic meson-field theory, *Z. Phys. A* **323**, 13 (1986).

[82] G. A. Lalazissis, J. König, and P. Ring, New parametrization for the lagrangian density of relativistic mean field theory, *Phys. Rev. C* **55**, 540 (1997).

[83] B. Sun, S. Bhattachiprolu, and J. M. Lattimer, Compiled properties of nucleonic matter and nuclear and neutron star models from nonrelativistic and relativistic interactions, *Phys. Rev. C* **109**, 055801 (2024).

[84] G. A. Lalazissis, T. Nikšić, D. Vretenar, and P. Ring, New relativistic mean-field interaction with density-dependent meson-nucleon couplings, *Phys. Rev. C* **71**, 024312 (2005).

[85] B. K. Agrawal, S. Shlomo, and V. K. Au, Determination of the parameters of a skyrme type effective interaction using the simulated annealing approach, *Phys. Rev. C* **72**, 014310 (2005).

[86] N. Van Giai and H. Sagawa, Spin-isospin and pairing properties of modified skyrme interactions, *Phys. Lett. B* **106**, 379 (1981).

[87] B. K. Agrawal, S. Shlomo, and V. Kim Au, Nuclear matter incompressibility coefficient in relativistic and nonrelativistic microscopic models, *Phys. Rev. C* **68**, 031304 (2003).

[88] E. Chabanat, P. Bonche, P. Haensel, J. Meyer, and R. Schaeffer, A Skyrme parametrization from subnuclear to neutron star densities, *Nuc. Phys. A* **627**, 710 (1997).

[89] E. Chabanat, P. Bonche, P. Haensel, J. Meyer, and R. Schaeffer, A Skyrme parametrization from subnuclear to neutron star densities Part II. Nuclei far from stabilities, *Nuc. Phys. A* **635**, 231 (1998).

[90] P.-G. Reinhard and H. Flocard, Nuclear effective forces and isotope shifts, *Nuclear Physics A* **584**, 467 (1995).

[91] X. Roca-Maza, G. Colò, and H. Sagawa, New skyrme interaction with improved spin-isospin properties, *Phys. Rev. C* **86**, 031306 (2012).

[92] F. Douchin and P. Haensel, A unified equation of state of dense matter and neutron star structure, *Astron. Astrophys.* **380**, 151 (2001).

[93] G. Baym, C. Pethick, and P. Sutherland, The Ground State of Matter at High Densities: Equation of State and Stellar Models, *Astrophys. J.* **170**, 299 (1971).

[94] R. P. Feynman, N. Metropolis, and E. Teller, Equations of State of Elements Based on the Generalized Fermi-Thomas Theory, *Phys. Rev.* **75**, 1561 (1949).

[95] B.-J. Cai and L.-W. Chen, Nuclear matter fourth-order symmetry energy in the relativistic mean field models, *Phys. Rev. C* **85**, 024302 (2012).

[96] N. Paar, C. C. Moustakidis, T. Marketin, D. Vretenar, and G. A. Lalazissis, Neutron star structure and collective excitations of finite nuclei, *Phys. Rev. C* **90**, 011304 (2014).

[97] V. Doroshenko, V. Suleimanov, G. Pühlhofer, and A. Santangelo, A strangely light neutron star within a supernova remnant., *Nat. Astron.* **6**, 1444–1451 (2022).

[98] D. Choudhury *et al.*, A NICER View of the Nearest and Brightest Millisecond Pulsar: PSR J0437–4715, *Astrophys. J. Lett.* **971**, L20 (2024).

[99] T. Salmi *et al.*, A NICER View of PSR J1231-1411: A Complex Case, *Astrophys. J.* **976**, 58 (2024).

[100] B. P. Abbott *et al.* (LIGO Scientific Collaboration and Virgo Collaboration), Properties of the Binary Neutron Star Merger GW170817, *Phys. Rev. X* **9**, 011001 (2019).

[101] P. Koliogiannis, E. Yüksel, T. Ghosh, and N. Paar, Dipole Polarizability of Finite Nuclei as a Probe of Neutron Stars, *Astrophys. J. Lett.* **996**, L18 (2025).

[102] N. Paar, D. Vretenar, E. Khan, and G. Colò, Exotic modes of excitation in atomic nuclei far from stability, *Rep. Prog. Phys.* **70**, R02 (2007).

[103] X. Roca-Maza, M. Brenna, G. Colò, M. Centelles, X. Viñas, B. K. Agrawal, N. Paar, D. Vretenar, and J. Piekarewicz, Electric dipole polarizability in ^{208}Pb : Insights from the droplet model, *Phys. Rev. C* **88**, 024316 (2013).

[104] N. Paar, P. Ring, T. Nikšić, and D. Vretenar, Quasiparticle random phase approximation based on the relativistic Hartree-Bogoliubov model, *Phys. Rev. C* **67**, 034312 (2003).

- [105] G. Colò, L. Cao, N. Van Giai, and L. Capelli, Self-consistent RPA calculations with Skyrme-type interactions: The `skyrme_rpa` program, *Comp. Phys. Comm.* **184**, 142 (2013).
- [106] G. Colò and X. Roca-Maza, *User guide for the hfbcslqrpa(v1) code* (2021), [arXiv:2102.06562 \[nucl-th\]](https://arxiv.org/abs/2102.06562).
- [107] P.-G. Reinhard and W. Nazarewicz, Information content of a new observable: The case of the nuclear neutron skin, *Phys. Rev. C* **81**, 051303 (2010).
- [108] C. D. Capano *et al.*, Stringent constraints on neutron-star radii from multimessenger observations and nuclear theory, *Nat. Astron.* **4**, 625 (2020).
- [109] T. Dietrich *et al.*, Multimessenger constraints on the neutron-star equation of state and the Hubble constant, *Sci.* **370**, 1450 (2020).